Origins of the Decadal Predictability of East Asian Land Summer Monsoon Rainfall

JUAN LI AND BIN WANG

Earth System Modeling Center, Nanjing University of Information Science and Technology, Nanjing, China, and Department of Atmospheric Sciences, and International Pacific Research Center, University of Hawai'i at Mānoa, Honolulu, Hawaii

(Manuscript received 18 November 2017, in final form 4 February 2018)

ABSTRACT

The present study aims to explore the origins of decadal predictability of East Asian land summer monsoon rainfall (EA-LR) and estimate its potential decadal predictability. As a preliminary study, a domain-averaged EA-LR index (EA-LI) is targeted as it represents the leading mode of variability reasonably well. It is found that the decadal variations of EA-LI are primarily linked to a cooling over the central-eastern tropical Pacific (CEP) and a warming over the extratropical North Pacific and western tropical Pacific (NWP) during May–October. Two numerical experiments suggest that the CEP cooling may be a major driver of EA-LR, while the NWP warming, which is largely a response, cannot be treated as a forcing to EA-LR. However, this does not mean that the NWP sea surface temperature anomalies (SSTAs) play no role. To elaborate on this point, a third experiment is conducted in which the observed cooling is nudged in the CEP but the SST is nudged to climatology in the NWP (i.e., atmosphere–ocean interaction is not allowed). The result shows anomalous northerlies and decreased rainfall over East Asia. Results of the three experiments together suggest that both the forcings from the CEP and the atmosphere–ocean interaction in the NWP are important for EA-LR. Assuming that the tropical and North Pacific SSTAs can be ''perfectly'' forecasted, the so-called perfect prediction of EA-LI, which is achieved by a physics-based empirical model, yields a significant temporal correlation coefficient skill of 0.70 at a 7–10-yr lead time during a 40-yr independent hindcast (1968–2009), providing an estimation of the lower bound of potential decadal predictability of EA-LI.

1. Introduction

Long-term adaptation to and mitigation policies against the impact of climate change require skillful decadal climate prediction, which could provide useful information for policymakers and stakeholders to make decisions one or several decades in advance. Thus, decadal climate predictions have received increasing attention (Smith et al. 2007; Meehl et al. 2009; van Oldenborgh et al. 2012; Bellucci et al. 2015; Meehl et al. 2014; Wang et al. 2018). Dynamical decadal prediction from the phase 5 of the Coupled Model Intercomparison Project (CMIP5) multimodel ensemble shows a greater skill for temperature over most parts of the ocean (Kim et al. 2012; van Oldenborgh et al. 2012; Meehl et al. 2014) but poor skills for precipitation over land (Meehl et al. 2014).

Changes of monsoon rainfall, especially the changes over land area with large human populations, are of great societal and scientific importance. The East Asian summer monsoon (EASM) is a unique component of the global monsoon system (Wang and Ding 2006); it possesses specific characteristics due to local land–sea thermal contrast, topography, and feedbacks among distinct components of the climate system (Tao and Chen 1987; Lau et al. 1988; Wang et al. 2000; Wang and Zhang 2002; Wang and Li 2004; Ding et al. 2008; Wang et al. 2008a; Ha et al. 2012; Zhu Z. et al. 2012). The EASM has large decadal variability as well as interannual variability. It has been shown that the EASM experienced pronounced decadal changes in the late 1970s (Hu 1997; Chang et al. 2000; Wu and Wang 2002) and mid-1990s (Kwon et al. 2007; Yim et al. 2014a; Zhu et al. 2014), but prediction of decadal variability of East Asian land summer monsoon rainfall (EA-LR) remains an unexplored frontier and an outstanding challenge.

Decadal climate variability is controlled by both internal variability and anthropogenic forcing (Hawkins and Sutton 2009; Meehl et al. 2009; Solomon et al. 2011; Goddard et al. 2012; Sun et al. 2013). Many studies have put forward that decadal variability of the EASM is closely related to natural internal forcing (Zhou et al. 2009a;

Denotes content that is immediately available upon publication as open access.

Corresponding author: Bin Wang, wangbin@hawaii.edu

DOI: 10.1175/JCLI-D-17-0790.1

Zhang 2015). A variety of speculations and hypotheses have been proposed along this line of thinking. It has been suggested that the change of sea surface temperature (SST) and convective activity over the tropical Indian Ocean and western Pacific leads to the decadal westward extension of the western Pacific subtropical high (WPSH), thus further modulating decadal change of the EASM (Hu 1997; Chang et al. 2000; Gong and Ho 2002; Yang and Lau 2004; Zhang et al. 2008; Zhou et al. 2009b). Wang et al. (2008b) proposed that the strengthening relationships between El Niño–Southern Oscillation (ENSO) and the western North Pacific, East Asian, and Indonesian monsoons since the late 1970s are attributed to the increased magnitude and periodicity of ENSO and the strengthened monsoon–ocean interaction. The SST warming over tropical oceans, especially over the central and eastern Pacific, has been speculated to play a major role in weakening the EASM during the recent decades (Li et al. 2010; Park et al. 2010). The phase of Pacific decadal oscillation is found to be influential in decadal variation of the EASM (Yoon and Yeh 2010; Feng et al. 2014; Yu et al. 2015). In addition, Lopez et al. (2016) showed that the Atlantic meridional overturning circulation (AMOC) plays a key role in modulating decadal variability of the EASM as well as other Northern Hemisphere monsoons, and in Northern Hemisphere monsoon regions the Hadley circulation and monsoons show significant responses to the AMOC decadal variability. Eurasian snow cover and Arctic sea ice in spring may influence decadal EASM patterns via forcing the atmospheric circulation (Zhang et al. 2008; Wu et al. 2009). The heat source variation over the Tibetan Plateau could also partly contribute to EASM changes in the recent decades (Ding et al. 2009; Zhao et al. 2010; Duan et al. 2013; Liu et al. 2012). Most of the above studies focus on the decadal change of the EASM after 1950s or 1960s due to short records or sparse spatial coverage. Decadal variation of the EASM in the longer term has been rarely investigated.

The effects of anthropogenic factors on decadal variability of the EASM remain uncertain. It is found that the EASM can be weakened by increased aerosols across East Asia (Menon et al. 2002; Qian et al. 2009; T. Wang et al. 2013; Song et al. 2014) and global warming driven by greenhouse gases (Ueda et al. 2006; C. Zhu et al. 2012). But these conclusions largely depend on the sensitivity of the climate models to greenhouse gases and aerosol forcings. On decadal time scales, although regional anthropogenically forced changes can be expected, the changes are typically smaller than those arising from internal variability (Murphy et al. 2010; Wang et al. 2012; B. Wang et al. 2013).

The mechanisms of decadal change of EASM are widely studied. However the decadal prediction of the EASM is seldom explored. The skill of decadal predictions can be improved with a better understanding of the related physical mechanisms, especially the process of the natural decadal variability. Establishing a physics-based empirical prediction model (P-E model) that takes into account physical mechanisms is a useful way to predict various meteorological phenomena (Lee et al. 2011; Xing et al. 2016; Yim et al. 2014b; Wang et al. 2015a,b; Grunseich and Wang 2016; Li and Wang 2016; Zhu and Li 2017). It has been shown that the physical basis of the entire Northern Hemisphere land monsoon rainfall is primarily rooted in the multidecadal oscillation of a dipole SST pattern between the North Atlantic and the south Indian Ocean (Wang et al. 2018). Besides, it also has a complementary source from an east–west thermal contrast in the Pacific (Wang et al. 2018).

What physical processes are critical to the decadal predictability of EA-LR? In this study our objectives are to find out the predictability sources of decadal variability of EA-LR during the past 112 years, to understand the physical processes related to the predictability sources by performing numerical experiments, and finally to build P-E models to estimate the potential decadal predictability of EA-LR.

Following this introduction, section 2 describes the data, methodology, and the coupled climate model. In section 3, a grand EA-LR index is defined and its decadal predictability sources are explored. The physical linkage between predictability sources and EA-LR is testified by numerical experiments in section 4. The assessment of the potential decadal predictability of EA-LI is presented in section 5. The last section provides concluding remarks and discussion.

2. Data and methodology

a. Data

Monthly precipitation is derived from two datasets with long instrumental records: the Climatic Research Unit (CRU) TS3.21 dataset on a 0.5° × 0.5° grid during 1901–2012 (Harris et al. 2014) and the twentieth-century reconstructed precipitation dataset with a horizontal resolution of 2.5° × 2.5° for 1901–2010 (Smith et al. 2010). The arithmetic mean of these two datasets is used as observed precipitation. Monthly SST is obtained from the arithmetic mean of two datasets: the Hadley Centre Sea Ice and Sea Surface Temperature dataset (HadISST) (Rayner et al. 2003) with a horizontal resolution of 1° × 1° and the National Oceanic and Atmospheric Administration extended reconstructed SST (ERSST) version 3 (Smith et al. 2008) with 2° × 2° resolution for 1901–2012. The sea level pressure (SLP) and 850-hPa winds on a 2° × 2° grid are derived from the Twentieth Century Reanalysis

TABLE 1. Description of numerical experiments. Each experiment contains 30 ensemble members. The control run (CTRL) is a free coupled run.

Experiment	Description
EXP_CEP1 (2)	CTRL but nudging by predictor SSTAs (–SSTAs) in the CEP (20°S–30°N, 180°–80°W) from May to October.
EXP_NWP1 (2)	CTRL but nudging by predictor SSTAs (–SSTAs) in the NWP (25°–50°N, 120°E–140°W and 20°–25°N, 120°–160°E) from May to October.
EXP_CNP1 (2)	CTRL but nudging by climatological SST in the NWP and predictor SSTAs (–SSTAs) in the CEP from May to October.

data for the period 1901–2012 (Compo et al. 2011). All datasets are interpolated to a uniform resolution of 2.5° × 2.5° to make spatial resolutions comparable.

Three coupled climate models that participated in CMIP5 (Taylor et al. 2012) are employed to estimate the dynamical prediction skills of decadal variations of EA-LR. These three models are the Hadley Centre coupled global climate model, version 3 (HadCM3), the Geophysical Fluid Dynamics Laboratory Climate Model version 2.1 (GFDL-CM2.1) and the Max Planck Institute Earth System Model, low resolution (MPI-ESM-LR). The MPI-ESM-LR has three ensemble members, while HadCM3 and GFDL-CM2.1 have 10 members. The hindcasts consist of 51 sets of 10-yr retrospective predictions that are initialized every year from 1961 to 2011. Dynamic prediction skills in this study are all based on the three models' multimodel ensemble (MME). The MME mean is constructed with equal weights.

In this study, the 4-yr running mean (referred to as the decadal component) is applied to both observations and the dynamical hindcast. It is a widely used approach to filter out high-frequency components in assessment of decadal prediction (Kim et al. 2012; van Oldenborgh et al. 2012; Goddard et al. 2013). Taking autocorrelations into account, all statistical tests for correlation coefficients are determined by the effective degrees of freedom (Livezey and Chen 1983).

b. Coupled climate model and nudging method

The Nanjing University of Information Science and Technology (NUIST) coupled Earth System Model (NUIST-ESM) v1a (Cao et al. 2015) is used to conduct numerical experiments in this study. The atmospheric component of this coupled model is ECHAM v5.3 (Roeckner et al. 1996) with a horizontal resolution of around 2.8° × 2.8° in longitude and latitude and 31 levels in vertical. The Nucleus for European Modeling of the Ocean (NEMO) (Madec 2008) with a 2° × 2° horizontal resolution and 31 vertical levels is applied as the oceanic component model, while the sea ice component model is version 4.1 of the Los Alamos Sea Ice Model (CICE) (Hunke and Lipscomb 2010). The annual mean, annual cycle, monsoon variability, and ENSO can be reproduced realistically by NUIST-ESM (Cao et al. 2015).

Sensitivity experiments are conducted with SST nudging in given regions. The model includes a nudging term that adjusts a model field toward the observed (or target) field (Hoke and Anthes 1976). The model-simulated SST is nudged to approach the observed SST anomalies (SSTAs) superposed on the model climatology by adding an additional SST tendency term ($\partial \mathrm{SST}/\partial t$). The SST tendency term is defined as

$$\frac{\partial \mathrm{SST}}{\partial t} = (\mathrm{SST}_{\mathrm{mc}} + \Delta\mathrm{SST} - \mathrm{SST}_m)/86400,$$

where $\mathrm{SST}_{\mathrm{mc}}$ indicates the climatological SST in the control run, ΔSST is the observed SSTAs regressed onto predictor, and SST_m represents the model-simulated SST in each time step. The nudging time interval is one day (86 400 s). Paired experiments are performed with positive ΔSST in one and negative ΔSST in the other. The ΔSST values are triple the observed counterparts of the regressed SSTAs. The use of tripled SST and positive ΔSST minus negative ΔSST difference leads to an exaggeration of the SST-produced signal. Each experiment consists of 30 ensemble members. The differences of the ensemble means of these two experiments are identified as the response to the nudged SSTAs. For instance, the predictor SSTAs in the tropical central-eastern Pacific (20°S–30°N, 180°–80°W) from May to October are used as ΔSST for EXP_CEP1 (Table 1; Fig. 6a). EXP_CEP2 is the same as EXP_CEP1, but it adopts the opposite sign of SSTAs as SST nudging anomalies (−ΔSST). The difference between the ensemble means of EXP_CEP1 and EXP_CEP2 is identified as the response (Fig. 7).

c. Methodology for establishing the P-E model

The P-E model is established based on physical relationships between the predictor and predictand (Wang et al. 2015b). First, simultaneous correlation maps between the predictand and SST are used to identify potential physically meaningful "predictors." Then, the stepwise regression is used to build the P-E model, in

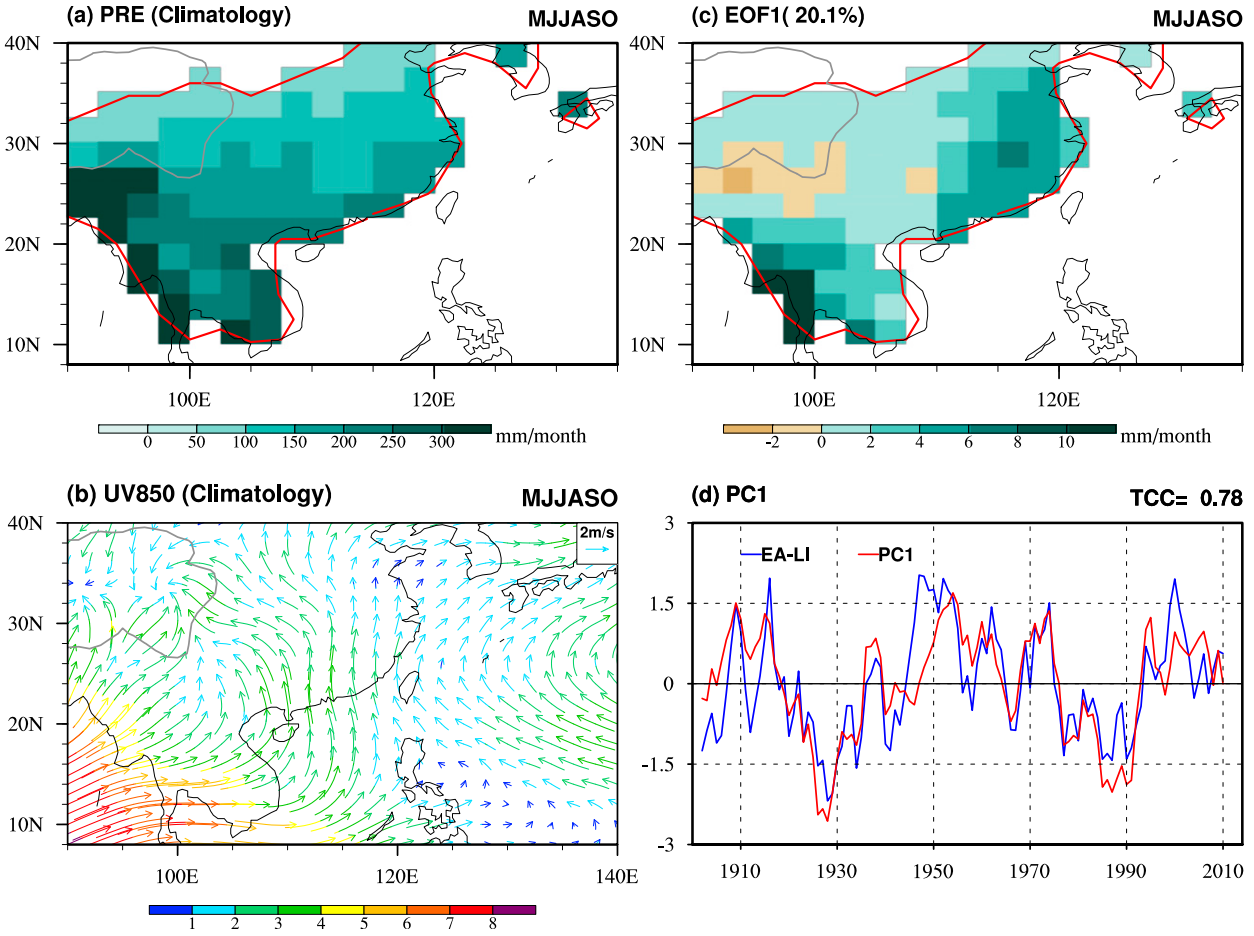

FIG. 1. Climatological mean (a) precipitation and (b) 850-hPa winds for MJJASO during 1901–2012, and the (c) spatial pattern and the (d) corresponding principal component of the first EOF mode of the local summer rainfall over East Asian land monsoon regions. For comparison, the East Asian land summer monsoon rainfall index (EA-LI) is also plotted in (d). The East Asian land monsoon domain is outlined by red curves in (a) and (c). The gray curves in (a)–(c) outline the location of the Tibetan Plateau. The detrended data are used to perform EOF analysis. A 4-yr running mean is applied in (c) and (d). The year in (d) represents the second year of the 4-yr running mean. For example, the value for 1902 is the average for the period of 1901–04.

which important predictors can be identified and mutually independent predictors are considered. Taking the simultaneous correlation into account, the predictor is defined in a large box area to focus on large-scale signals (Lee et al. 2013). The predictors are defined by

$$\text{Pred}\,(t) = [\text{SST}\,(t, \text{lat}, \text{lon})\text{TCC}\,(\text{lat}, \text{lon})],$$

where TCC is the temporal correlation coefficient between the predictand and SST values during the training period (1901–60). Square brackets are the areal mean over the selected regions.

Other than TCC, the mean square skill score (MSSS) is chosen as a deterministic verification metric (Murphy 1988; WMO 2002; Goddard et al. 2013). The MSSS is essentially the differences between the mean square error (MSE) of the forecast and the MSE of the climatology. A positive (negative) MSSS indicates that the forecast is better (worse) than climatology.

3. Grand EA-LR index and its decadal predictability sources

Monsoon precipitation domains are defined by a local summer-minus-winter precipitation rate exceeding 2 mm day^{-1} and local summer precipitation exceeding 55% of the annual total rainfall (Wang et al. 2012). The EA-LR domain is outlined by red curves in Fig. 1a. May to October (MJJASO) is taken as local summer since the rainy season generally starts in May and ends in October over Southeast and East Asia (Wang and LinHo 2002) and the climatological annual cycle has broad peaks from May to October. The climatology of EASM features low-level southwesterlies over the

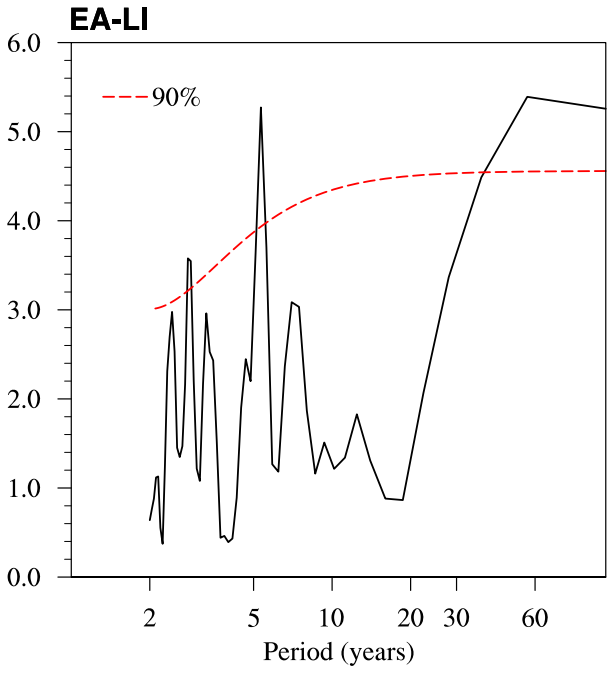

FIG. 2. Spectra of yearly summer (MJJASO) mean EA-LI obtained by averaging three periodogram bins (bandwidth: 40).

Indo-China region and southerlies along the west flank of WPSH that bring abundant moisture into the EASM region (Fig. 1b), forming major rainbands over the Indo-China Peninsula and eastern China (Fig. 1a).

To facilitate prediction and study the variability of EA-LR, a grand EA-LR index (EA-LI) is defined as the MJJASO precipitation averaged over the grand EA (10°–40°N, 90°–135°E) land monsoon domain (Fig. 1a).

Is the area-averaged rainfall index a meaningful measure for EA-LR variability? To address this question, we examine the leading empirical orthogonal function (EOF) mode of rainfall variability. On decadal time scales, the first EOF mode of detrended local summer rainfall over the grand EA land monsoon domain shows a nearly uniform spatial pattern and accounts for 20% of the total variance (Fig. 1c). Meanwhile, the decadal component of EA-LI is well correlated (TCC = 0.78) with the corresponding leading principal component (Fig. 1d). Therefore, the decadal EA-LI is appropriate for describing the decadal variability of the major mode of EA-LR. Caution should be exercised as EA-LI may not well represent the precipitation over the small area in the south of the Tibetan Plateau because the spatial pattern of the leading mode there shows an opposite sign. In addition, the spectral analysis of yearly EA-LI also suggests a significant energy rise on a multidecadal time scales (Fig. 2).

Note that the grand EA domain (10°–40°N, 90°–135°E) in the present study is different from the traditional EA domain (10°–50°N, 105°–135°E). Because of the domain dependence of EOF analysis, the leading EOF pattern here (Fig. 1c) is not dominated by a north–south dipole pattern as shown by the leading EOF pattern for the traditional EA domain (figure not shown).

What is the physical basis for decadal prediction of EA-LR? To unravel predictability sources of decadal variability of EA-LR, we analyze how EA-LI links to simultaneous global lower boundary anomalies (i.e., SST, SLP, 850-hPa wind, and precipitation). As shown in Fig. 3, the intensified EA-LR is related to an extended La Niña SST pattern and strengthened subtropical high over the Pacific. The associated low pressure extending from the Ganges River valley to central East Asia (EA) (Fig. 3b) thereby favors the convergence and monsoon rainfall over there. Meanwhile, the high SLP anomalies stretching from the northern South China Sea to southern Okhotsk may enhance the southerlies along the coast of EA (Fig. 3b), which bring a large amount of water vapor from the tropical western Pacific, leading to strengthened rainfall over EA (Fig. 3a).

What is the primary lower boundary forcing in modulating decadal variability of EA-LR? Simultaneous tropical North Pacific (TNP) SSTAs (black box in Fig. 3; 20°S–60°N, 120°E–80°W) are identified as a main forcing, which feature cooling over the central-eastern tropical Pacific (CEP) and warming over the midlatitude North Pacific and western tropical Pacific (NWP) from May to October (Fig. 3a). Thus, the TNP index (TNPI) can be obtained as a predictor as defined in section 2c. Figure 4 also indicates that the decadal variation of EA-LI is significantly correlated to the corresponding decadal variation of TNPI at a 95% confidence level.

To confirm the possible effects of the TNP SSTAs, the lower boundary anomalies correlated with the TNPI are further examined. The accompanying SLP contrast between WPSH and the Southeast Asian continent low, as well as the southerly anomalies along the coast of EA, suggests that the TNP SSTAs could be a forcing to convection over EA (Fig. 5).

4. Physical linkage between TNP SSTAs and EA-LR

How do the CEP cooling and NWP warming influence the EA-LR anomalies? Previous studies have revealed that the remote forcing from the CEP SST is the major cause for variability of EASM (Wang et al. 2000; Wang

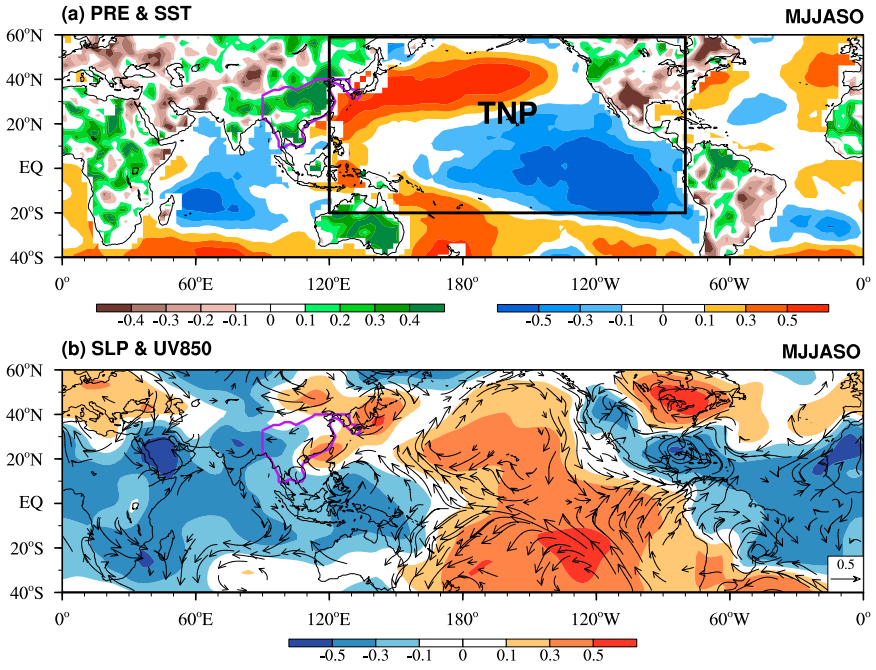

FIG. 3. Simultaneous (MJJASO) correlation coefficient map of (a) precipitation (shading over land) and SST (shading over ocean) and (b) SLP (shading) and 850-hPa winds (vectors) with reference to EA-LI using data from 1901 to 1960. A 4-yr running mean is applied. The black box indicates the region for TNP. The EA-LR domain is outlined by purple curves.

et al. 2003), and warm pool SSTAs during local summer season are a result of atmosphere–ocean interaction and cannot be treated as a forcing to the atmosphere (Wang et al. 2004; Wang et al. 2005; Wu and Kirtman 2005). Thus, three sets of coupled model experiments are designed to testify the causative linkage between the TNP SSTAs and EA-LR. 1) We nudge the predictor-related SSTAs in the CEP (Fig. 6a) in the first set of experiments (EXP_CEP1 and EXP_CEP2; Table 1). This design treats the CEP SSTAs as a forcing while SSTAs outside of this area are determined by atmosphere–ocean interaction. 2) Then we nudge the predictor related SSTAs in the NWP (Fig. 6b) in the second set of experiments (EXP_NWP1 and EXP_NWP2; Table 1) to test whether NWP SSTAs are a forcing. 3) If NWP SSTAs are not a forcing, is air–sea interaction in the NWP important? To identify the role of air–sea interaction in the NWP in modulating EA-LR, we design the third set of experiments (EXP_CNP1 and EXP_CNP2; Table 1) in which SST in the NWP is nudged to the climatological value (without air–sea interaction) while the CEP SSTA forcing is retained (Fig 6c). For each experiment the nudging is only applied from May to October. The shading in Fig. 6 shows the regions of SSTA nudging (i.e., ΔSST) in May; patterns of SSTA nudging from June to October are similar to those in May except for gradually intensified amplitudes.

With the negative SSTAs from May to October over the CEP (Fig. 6a), the results from the coupled model simulations (EXP_CEP1 minus EXP_CEP2) basically resemble the observed features, that is, anomalous easterlies over the western tropical Pacific, enhanced subtropical high, and intensified rainfall over southern EA (Fig. 7). It is therefore demonstrated that La Niña SSTAs drive the EA-LR variability through the associated changes in Walker circulation and enhanced Pacific subtropical high resulting from a Rossby-wave response (Gill 1980; Wang et al. 2000). But the rainfall over central EA is underestimated in the simulation (Fig. 7a). Note that the SST warming over the midlatitude North Pacific can be simulated (Fig. 7b), which implies that the CEP cooling could generate this extratropical SST

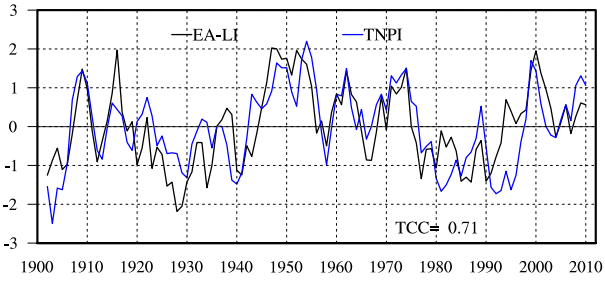

FIG. 4. Time series of observed decadal EA-LI and predictor TNPI.

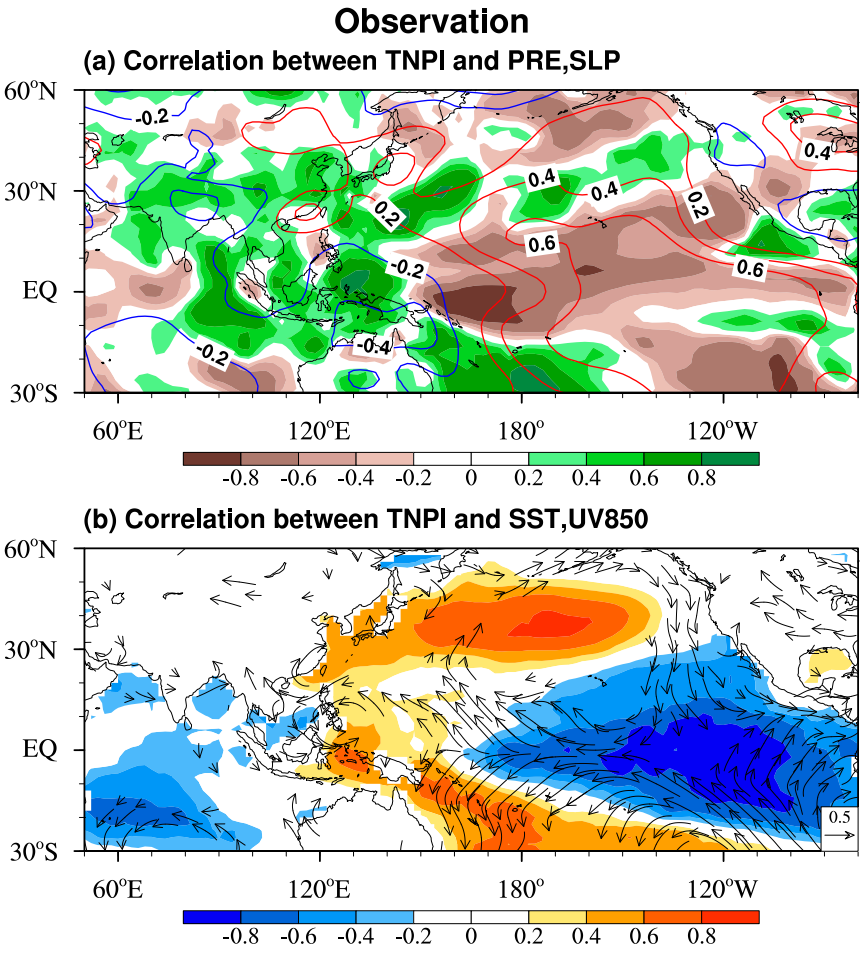

FIG. 5. Observed correlations maps of (a) MJJASO precipitation (shading), SLP (contours), (b) SST (shading), and 850-hPa winds (vectors) with reference to TNPI using data from 1901 to 1960. A 4-yr running mean is applied.

warming through an atmospheric bridge (Lau and Nath 1996) and local atmosphere–ocean interaction.

Can the NWP SSTAs be treated as a forcing? The results of the second pair of coupled model experiments (EXP_NWP1 minus EXP_NWP2) show that the positive NWP SSTA-induced (Fig. 6b) summer circulation is characterized by low SLP anomalies over the North Pacific as well as northerly anomalies along the coast of EA (Fig. 8), which are inconsistent with observed anomalies related to the SSTA predictor (Fig. 5), suggesting that the NWP SST warming cannot be regarded as a forcing to EA-LR; instead, it is a result of local atmosphere–ocean interaction. This does not mean that the NWP SSTAs are unimportant, because they can feed back to the atmosphere through an interactive mode.

Is air–sea interaction in the NWP important to EA-LR? The results of the third pair of coupled climate model experiments (EXP_CNP1 minus EXP_CNP2) are characterized by a strong cyclonic circulation and active convection over the western Pacific, northerly anomalies along the coast of EA, and reduced EA-LR (Fig. 9), which are different from the simulated results with atmosphere–ocean interaction in the NWP (Fig. 7) as well as observation (Fig. 5). It is suggested that, without local atmosphere–ocean interaction, the CEP SSTA forcing alone cannot reproduce observed EA-LR variability as well as observed anomalies over the NWP, implying that SSTAs in the NWP also have an impact on EA-LR through local atmosphere–ocean interaction.

The above three pairs of experiments thereby indicate that EA-LR variability originates from the CEP SSTAs, whereas SSTAs in the NWP are the result of a combined response to the CEP SSTA forcing and local atmosphere–ocean interaction. Note that SSTAs in the NWP are not a passive response to the atmospheric forcing. Instead, they also exert their influences on the atmosphere. Treating them as a forcing to the atmosphere is inadequate, but regarding them as

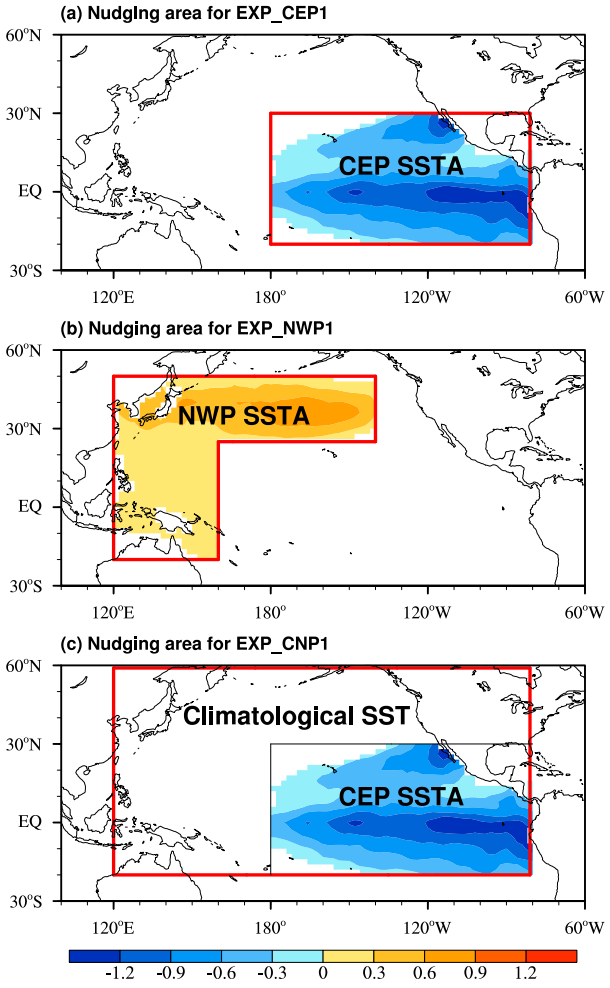

FIG. 6. Nudging area (red box) used in the coupled model experiments (a) EXP_CEP1, (b) EXP_NWP1, and (c) EXP_CNP1. Predictor SSTAs (ΔSST) in May are indicated by shading (units: K).

a slave to the atmosphere is also inappropriate. The EA-LR responds to TNP SSTAs as a whole, although the root cause is in the tropical central-eastern Pacific. That is the reason why the TNP SSTAs as a whole should be taken as a ''predictor.''

5. Potential decadal predictability of EA-LR

In order to investigate to what extent the EA-LI can be potentially predicted, the P-E model is established by using the ''perfect'' prediction approach, in which we assume that the predictor, TNPI, can be perfectly predicted (i.e., use observed values) by the dynamical model. The prediction skill derived from this ideal method (i.e., use observed values of predictors) provides an estimation of potential predictability (Kang and Shukla 2009).

To make a parallel comparison to dynamical models, we investigate the rolling-retrospective independent forecast with 10-yr forward prediction. In this method, 51 sets of 10-yr retrospective predictions are made to compare with CMIP5 dynamical models' decadal predictions, which are initialized every year from 1961 to 2011. Similar to dynamical decadal prediction, for prediction initialized in 1961, we establish a P-E prediction model using the data from 1901 to 1960, and then predicted the ensuing 10 years (1961–70); for prediction initialized in 1962, data from 1902 to 1961 are employed to build the prediction equation to forecast the following 10 years (1962–71); and so on. In total, 51 segments of 10-yr prediction are made from 1961 to 2011. Then 7 time series are obtained by averaging lead times of 1–4-, 2–5-, 3–6-, 4–7-, 5–8-, 6–9-, and 7–10-yr predictions, respectively. After applying a 4-yr running mean, the time series start from 1962 to 2009 for 1–4 yrlead time, 1963–2009 for 2–5 yr lead time, and so on to 1968–2009 for 7–10 yr lead time. Since the predictor is selected from the data for 1901–1960, the rolling-retrospective forecast can be considered as an independent forecast because no ''future'' (after the training period) information is used. The so-called perfect rolling-retrospective independent prediction for decadal EA-LI, which is made by the P-E model using observed TNPI, shows a significant TCC skill of 0.70 at 7–10-yr lead time during 1968–2009 (Fig. 10a), indicating that about 49% of the decadal variances of the EA-LI may be potentially captured by the TNPI 10 years ahead. This result may provide an estimate for the potential decadal predictability of EA-LR based on a perfect dynamically forecasted TNPI. The MSSS values made by this perfect prediction are larger than 0.37 for all lead times (Fig. 10b).

How does the coupled climate model perform in predicting decadal variability of EA-LI? Three models' MMEs, which are derived from the CMIP5 decadal experiment initialized every year in the period 1961–2011, are assessed. It is suggested that the decadal prediction of EA-LI has an insignificant TCC skill of 0.29 and a low MSSS of –0.44 at up to 7–10 years (Fig. 10). The persistent prediction skills are also poor (Fig. 10). Thus, there is large room for improving the decadal prediction of EA-LI.

6. Summary and discussion

Our objective for this study is to understand the sources of decadal predictability of EA-LR and estimate the potential predictability. The major findings are summarized as follows:

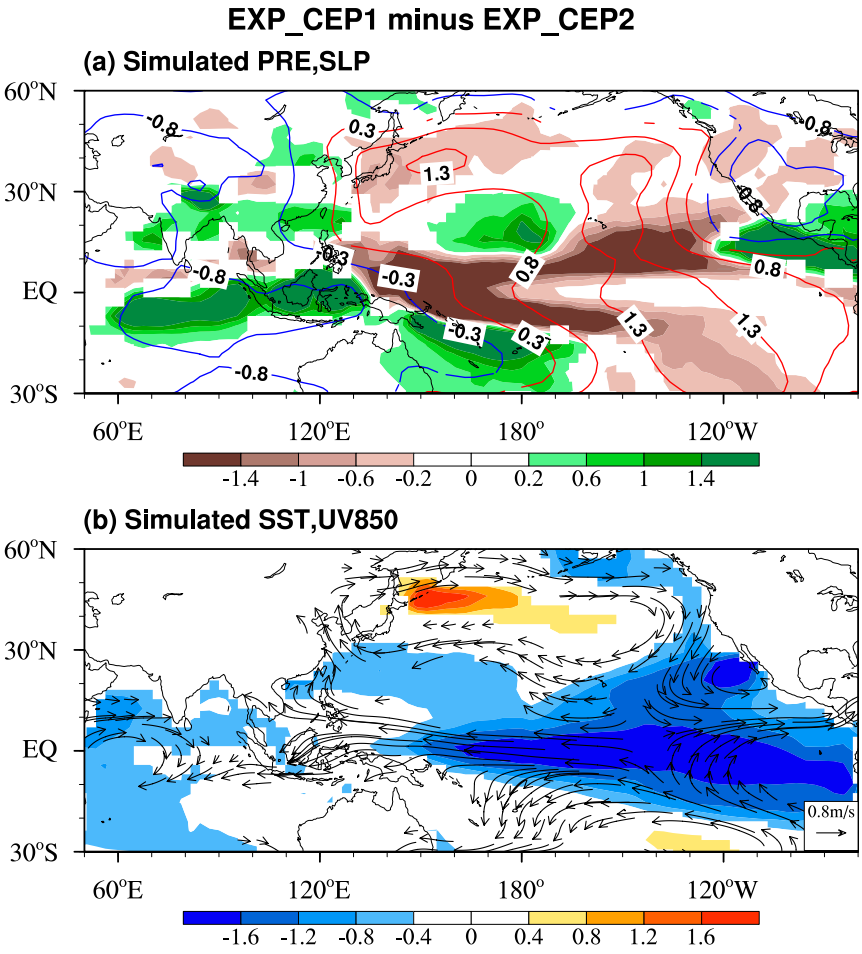

FIG. 7. Model simulated MJJASO responses (EXP_CEP1 minus EXP_CEP2) of (a) precipitation (shading; mm day^{-1}) and SLP (contours; hPa) and (b) SST (shading; K) and 850-hPa wind (vectors; m s^{-1}). Simulated fields that are significant at the 90% confidence level (Student's *t* test) are shown.

1) A grand area-averaged EA land rainfall index is defined. This is a meaningful measurement of EA-LR variability since the first EOF mode of EA-LR shows a nearly uniform spatial pattern and EA-LI is well correlated with the corresponding principal component on decadal time scales.
2) The physical basis of decadal prediction of EA-LR is revealed. The enhanced EA-LR is related to the extended La Niña SST pattern, high pressure over subtropical Pacific, low pressure over central Asia, and southerlies along the coast of EA, thereby increasing the moisture convergence and monsoon rainfall over EA. The summer TNP SSTAs, which are selected as a predictability source, characterize CEP cooling and NWP warming from May to October, accompanied by SLP contrast across the Southeast Asian continent low and WPSH, southerly anomalies along the coast of EA, and enhanced rainfall over EA.
3) To verify the causative physical linkage between the TNP SSTAs and EA-LR, three sets of paired numerical experiments are conducted by using coupled climate models. The first set of paired experiments (EXP_CEP1 and EXP_CEP2) with the CEP SSTA nudging demonstrates that La Niña SSTAs can enhance the Pacific subtropical high through Rossby wave response, resulting in strengthened southerlies along the coast of EA and intensified EA-LR. Thus, the CEP SSTAs can be considered as the main driver to EA-LR. The simulated variability of the mid-latitude North Pacific SSTAs turns out to be the responses forced by the CEP SSTAs. The second set of paired coupled model experiments (EXP_NWP1 and EXP_NWP2) with the NWP SSTA nudging shows opposite anomalies in contrast to observations, indicating that the NWP SST variability cannot be regarded as a forcing to EA-LR. However, it does

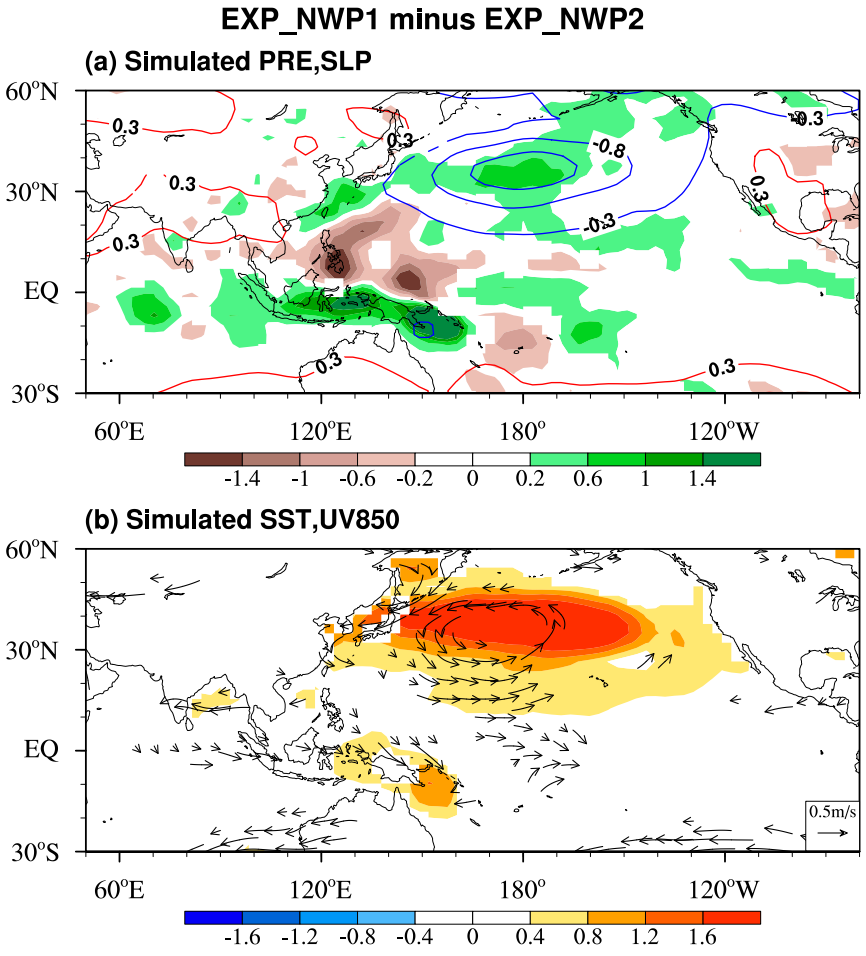

FIG. 8. Model-simulated MJJASO responses (EXP_NWP1 minus EXP_NWP2) of (a) precipitation (shading; mm day^{-1}) and SLP (contours; hPa) and (b) SST (shading; K) and 850-hPa wind (vectors; m s^{-1}). Simulated fields that are significant at the 90% confidence level (Student's *t* test) are shown.

not mean that the NWP is unimportant. Nudging SST in the NWP to the climatological value (without the air–sea interaction) while retaining the CEP SSTA forcing, the model responses from the third set of experiments (EXP_CNP1 and EXP_CNP2) hint that the SSTAs over the NWP also exert influence on EA-LR through local atmosphere–ocean interaction.

4) The potential decadal predictability of EA-LI is assessed. By using ''perfect'' dynamically forecasted (i.e., observed) TNPI, the P-E model is capable of capturing decadal EA-LI with a significant TCC skill of 0.70 and an MSSS of 0.41 at 7–10-yr lead time during 1968–2009. These high skills offer an estimate for potential decadal predictability of EA-LI based on so-called perfect predicted TNPI. The dynamical models' direct prediction skill and persistent prediction skill for decadal variability of EA-LI are far from the potential predictability limit, suggesting that there is large room for improving decadal prediction of EA-LI.

It is shown that the TNP SSTAs are the primary source of decadal predictability of EA-LR. However, the TNP SSTAs are obtained from simultaneous SST, and therefore a hybrid dynamical–empirical approach is proposed for actual decadal prediction of monsoon rainfall (Wang et al. 2018), in which the ''predictors'' are derived from dynamical models, and then these predictors are used to build the P-E model to further predict monsoon rainfall. Because of the imperfectness of the dynamical model predicted SST, the actual prediction skill will be lower than the potential predictability estimated with observed SST. The hybrid dynamical–empirical approach can produce better prediction skills if the predictors can be forecasted well. In other words, the dynamical prediction

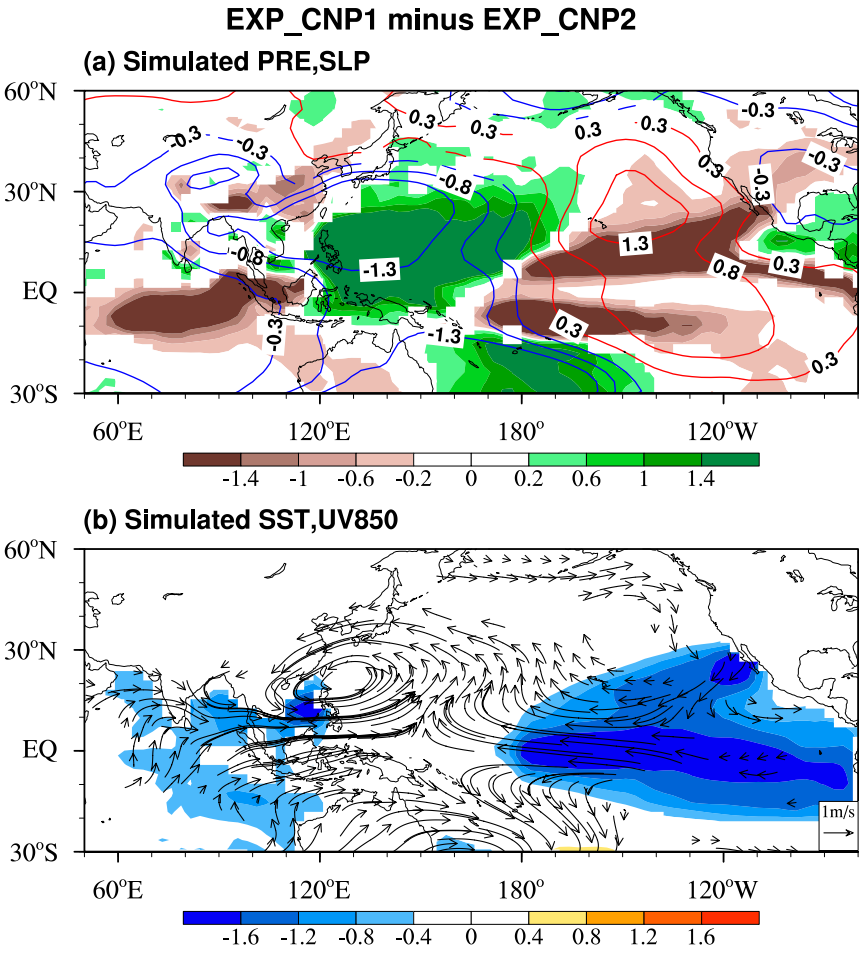

FIG. 9. Model-simulated MJJASO responses (EXP_CNP1 minus EXP_CNP2) of (a) precipitation (shading; mm day^{-1}) and SLP (contours; hPa) and (b) SST (shading; K) and 850-hPa wind (vectors; m s^{-1}). Simulated fields that are significant at the 90% confidence level (Student's *t* test) are shown.

skills for these predictors are critical to hybrid forecast. Because of the CMIP5 models' poor decadal prediction skills for North Pacific SST (Kim et al. 2014; Meehl et al. 2014), the hybrid forecast fails to predict decadal variability of EA-LI. Although in the present study the hybrid forecast method does not improve the decadal prediction skill for EA-LI, it still offers a promising path for decadal prediction in other regions provided that predictors can be well forecasted.

In addition, although the TNP SSTAs can yield high potential predictability, there are some caveats. The relationship between TNPI and EA-LI may experience secular changes (Fig. 11a). Their correlations were stable during the 1930s to 1970s but dropped in the recent four decades. Thus, continuously exploring and modifying the predictability sources is necessary. As shown in Fig. 11b, the cooling center over the eastern Pacific shifts northward during 1970–2012 from where it was during 1901–60 (Fig. 3a), which may be linked to the decreased correlations between TNPI and EA-LI in recent decades. Moreover, SST over the North Atlantic can be considered as a potential predictability source in the most recent 40 years (Fig. 11b), which may be a complement to TNPI.

How can the decadal prediction skill of EA-LR be improved? A direct method is to develop dynamical model physics of simulating precipitation. An alternative is to increase the dynamical prediction skill for the North Pacific SST through methods such as improving the initial conditions. Both approaches still need further study.

Acknowledgments. This study is supported by the Atmosphere–Ocean Research Center (AORC) and

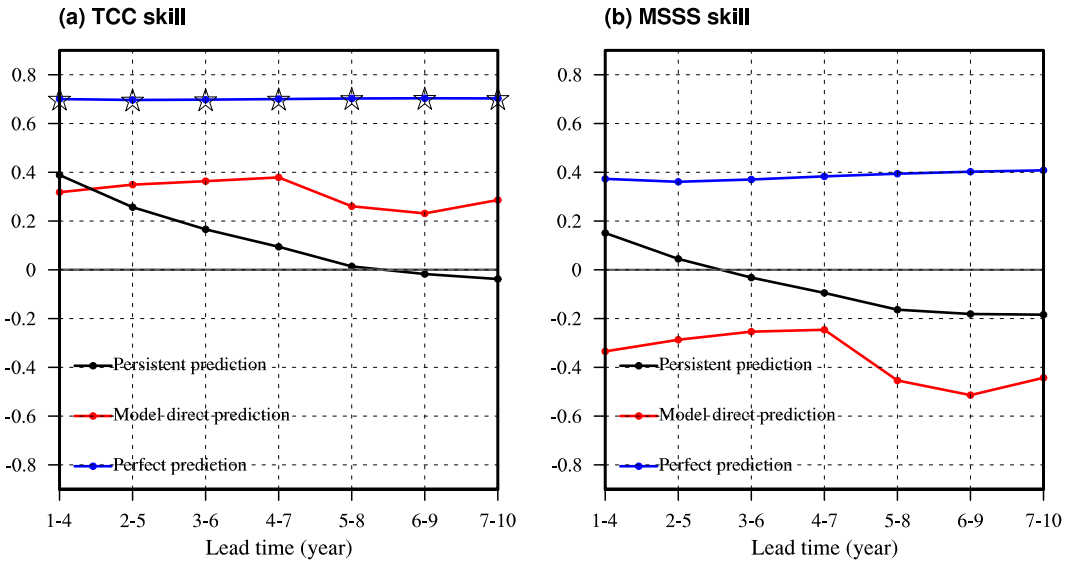

FIG. 10. Decadal hindcast skills for EA-LI. (a) TCC skill derived from "perfect" prediction (blue), model direct prediction (red), and persistent prediction (black) as functions of lead time (year) for the period of 1967–2011 (i.e., 4-yr running mean from 1968 to 2009). Stars indicate that the TCC is significant at a 95% confidence level taking serial autocorrelation into account. (b) As in (a), but for MSSS skill.

IPRC at the University of Hawaii, the National Research Foundation (NRF) of Korea through a Global Research Laboratory (GRL) grant of the Korean Ministry of Education, Science and Technology (MEST; 2011-0021927), the Startup Foundation for Introducing Talent of NUIST, and the Priority Academic Program Development (PAPD) of Jiangsu Higher Education Institutions. The AORC is partially funded by Nanjing University of Information Science and Technology (NUIST). This is NUIST–Earth System Modeling Center

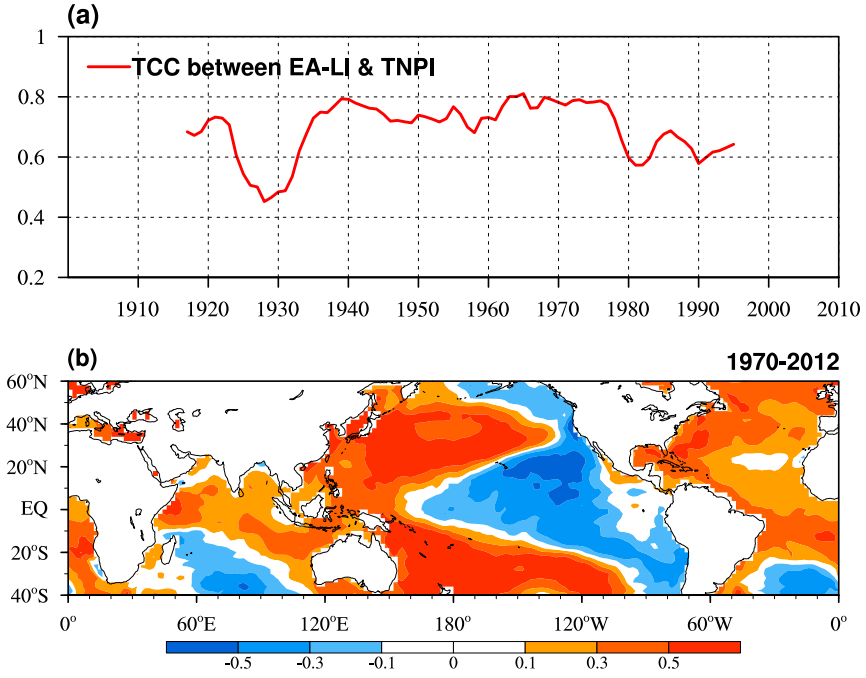

FIG. 11. (a) Time series of the 31-yr central sliding correlation coefficients between EA-LI and TNPI. (b) Simultaneous (MJJASO) correlation coefficient map of SST (shading over ocean) with reference to EA-LI using data from 1970 to 2012. A 4-yr running mean is applied.

(ESMC) Publication Number 208, SOEST Publication Number 10344, and IPRC Publication Number 1318.

REFERENCES

Bellucci, A., and Coauthors, 2015: An assessment of a multi-model ensemble of decadal climate predictions. *Climate Dyn.*, **44**, 2787–2806, https://doi.org/10.1007/s00382-014-2164-y.

Cao, J., B. Wang, B. Xiang, J. Li, T. Wu, X. Fu, and J. Min, 2015: Major modes of short-term climate variability in the newly developed NUIST Earth System Model (NESM). *Adv. Atmos. Sci.*, **32**, 585–600, https://doi.org/10.1007/s00376-014-4200-6.

Chang, C.-P., Y. Zhang, and T. Li, 2000: Interannual and interdecadal variations of the East Asian summer monsoon and tropical Pacific SSTs. Part I: Roles of the subtropical ridge. *J. Climate*, **13**, 4310–4325, https://doi.org/10.1175/1520-0442(2000)013<4310:IAIVOT>2.0.CO;2.

Compo, G. P., and Coauthors, 2011: The Twentieth Century Reanalysis project. *Quart. J. Roy. Meteor. Soc.*, **137**, 1–28, https://doi.org/10.1002/qj.776.

Ding, Y., Z. Wang, and Y. Sun, 2008: Inter-decadal variation of the summer precipitation in east China and its association with decreasing Asian summer monsoon. Part I: Observed evidences. *Int. J. Climatol.*, **28**, 1139–1161, https://doi.org/10.1002/joc.1615.

——, Y. Sun, Z. Wang, Y. Zhu, and Y. Song, 2009: Inter-decadal variation of the summer precipitation in China and its association with decreasing Asian summer monsoon Part II: Possible causes. *Int. J. Climatol.*, **29**, 1926–1944, https://doi.org/10.1002/joc.1759.

Duan, A., M. Wang, Y. Lei, and Y. Cui, 2013: Trends in summer rainfall over China associated with the Tibetan Plateau sensible heat source during 1980–2008. *J. Climate*, **26**, 261–275, https://doi.org/10.1175/JCLI-D-11-00669.1.

Feng, J., L. Wang, and W. Chen, 2014: How does the East Asian summer monsoon behave in the decaying phase of El Niño during different PDO phases? *J. Climate*, **27**, 2682–2698, https://doi.org/10.1175/JCLI-D-13-00015.1.

Gill, A. E., 1980: Some simple solutions for heat-induced tropical circulation. *Quart. J. Roy. Meteor. Soc.*, **106**, 447–462, https://doi.org/10.1002/qj.49710644905.

Goddard, L., J. W. Hurrell, B. P. Kirtman, J. Murphy, T. Stockdale, and C. Vera, 2012: Two time scales for the price of one (almost). *Bull. Amer. Meteor. Soc.*, **93**, 621–629, https://doi.org/10.1175/BAMS-D-11-00220.1.

——, and Coauthors, 2013: A verification framework for interannual-to-decadal predictions experiments. *Climate Dyn.*, **40**, 245–272, https://doi.org/10.1007/s00382-012-1481-2.

Gong, D.-Y., and C.-H. Ho, 2002: Shift in the summer rainfall over the Yangtze River valley in the late 1970s. *Geophys. Res. Lett.*, **29**, 1436, https://doi.org/10.1029/2001GL014523.

Grunseich, G., and B. Wang, 2016: Predictability of Arctic annual minimum sea ice patterns. *J. Climate*, **29**, 7065–7088, https://doi.org/10.1175/JCLI-D-16-0102.1.

Ha, K.-J., K.-Y. Heo, S.-S. Lee, K.-S. Yun, and J.-G. Jhun, 2012: Variability in the East Asian monsoon: A review. *Meteor. Appl.*, **19**, 200–215, https://doi.org/10.1002/met.1320.

Harris, I., P. D. Jones, T. J. Osborn, and D. H. Lister, 2014: Updated high-resolution grids of monthly climatic observations—The CRU TS3.10 dataset. *Int. J. Climatol.*, **34**, 623–642, https://doi.org/10.1002/joc.3711.

Hawkins, E., and R. Sutton, 2009: The potential to narrow uncertainty in regional climate predictions. *Bull. Amer. Meteor. Soc.*, **90**, 1095–1108, https://doi.org/10.1175/2009BAMS2607.1.

Hoke, J. E., and R. A. Anthes, 1976: The initialization of numerical models by a dynamic-initialization technique. *Mon. Wea. Rev.*, **104**, 1551–1556, https://doi.org/10.1175/1520-0493(1976)104<1551:TIONMB>2.0.CO;2.

Hu, Z.-Z., 1997: Interdecadal variability of summer climate over East Asia and its association with 500 hPa height and global sea surface temperature. *J. Geophys. Res.*, **102**, 19 403–19 412, https://doi.org/10.1029/97JD01052.

Hunke, E. C., and W. H. Lipscomb, 2010: CICE: The Los Alamos sea ice model documentation and software user's manual version 4.1. Los Alamos National Laboratory Tech. Rep. LA-CC-06-012, 76 pp.

Kang, I.-S., and J. Shukla, 2009: Dynamic seasonal prediction and predictability of the monsoon. *The Asian Monsoon*, B. Wang, Ed., Springer-Praxis, 585–612.

Kim, H.-M., P. J. Webster, and J. A. Curry, 2012: Evaluation of short-term climate change prediction in multi-model CMIP5 decadal hindcasts. *Geophys. Res. Lett.*, **39**, L10701, https://doi.org/10.1029/2012GL051644.

——, Y.-G. Ham, and A. A. Scaife, 2014: Improvement of initialized decadal predictions over the North Pacific Ocean by systematic anomaly pattern correction. *J. Climate*, **27**, 5148–5162, https://doi.org/10.1175/JCLI-D-13-00519.1.

Kwon, M., J.-G. Jhun, and K.-J. Ha, 2007: Decadal change in East Asian summer monsoon circulation in the mid-1990s. *Geophys. Res. Lett.*, **34**, L21706, https://doi.org/10.1029/2007GL031977.

Lau, K.-M., G. J. Yang, and S. H. Shen, 1988: Seasonal and intraseasonal climatology of summer monsoon rainfall over East Asia. *Mon. Wea. Rev.*, **116**, 18–37, https://doi.org/10.1175/1520-0493(1988)116<0018:SAICOS>2.0.CO;2.

Lau, N.-C., and M. J. Nath, 1996: The role of the "atmospheric bridge" in linking tropical Pacific ENSO events to extratropical SST anomalies. *J. Climate*, **9**, 2036–2057, https://doi.org/10.1175/1520-0442(1996)009<2036:TROTBI>2.0.CO;2.

Lee, J.-Y., B. Wang, Q. Ding, K.-J. Ha, J.-B. Ahn, A. Kumar, B. Stern, and O. Alves, 2011: How predictable is the Northern Hemisphere summer upper-tropospheric circulation? *Climate Dyn.*, **37**, 1189–1203, https://doi.org/10.1007/s00382-010-0909-9.

——, S.-S. Lee, B. Wang, K.-J. Ha, and J.-G. Jhun, 2013: Seasonal prediction and predictability of the Asian winter temperature variability. *Climate Dyn.*, **41**, 573–587, https://doi.org/10.1007/s00382-012-1588-5.

Li, H., A. Dai, T. Zhou, and J. Lu, 2010: Responses of East Asian summer monsoon to historical SST and atmospheric forcing during 1950–2000. *Climate Dyn.*, **34**, 501–514, https://doi.org/10.1007/s00382-008-0482-7.

Li, J., and B. Wang, 2016: How predictable is the anomaly pattern of the Indian summer rainfall? *Climate Dyn.*, **46**, 2847–2861, https://doi.org/10.1007/s00382-015-2735-6.

Liu, Y., G. Wu, J. Hong, B. Dong, A. Duan, Q. Bao, and L. Zhou, 2012: Revisiting Asian monsoon formation and change associated with Tibetan Plateau forcing: II. Change. *Climate Dyn.*, **39**, 1183–1195, https://doi.org/10.1007/s00382-012-1335-y.

Livezey, R. E., and W. Y. Chen, 1983: Statistical field significance and its determination by Monte Carlo techniques. *Mon. Wea. Rev.*, **111**, 46–59, https://doi.org/10.1175/1520-0493(1983)111<0046:SFSAID>2.0.CO;2.

Lopez, H., S. Dong, S.-K. Lee, and G. Goni, 2016: Decadal modulations of interhemispheric global atmospheric circulations and monsoons by the South Atlantic meridional overturning circulation. *J. Climate*, **29**, 1831–1851, https://doi.org/10.1175/JCLI-D-15-0491.1.

Madec, G., 2008: NEMO ocean engine. Institut Pierre-Simon Laplace (IPSL), Note du Pole de Modélisation Rep. 27, 396 pp.

Meehl, G. A., and Coauthors, 2009: Decadal prediction: Can it be skillful? *Bull. Amer. Meteor. Soc.*, **90**, 1467–1485, https://doi.org/10.1175/2009BAMS2778.1.

——, and Coauthors, 2014: Decadal climate prediction: An update from the trenches. *Bull. Amer. Meteor. Soc.*, **95**, 243–267, https://doi.org/10.1175/BAMS-D-12-00241.1.

Menon, S., J. Hansen, L. Nazarenko, and Y. Luo, 2002: Climate effects of black carbon aerosols in China and India. *Science*, **297**, 2250–2253, https://doi.org/10.1126/science.1075159.

Murphy, A. H., 1988: Skill scores based on the mean square error and their relationships to the correlation coefficient. *Mon. Wea. Rev.*, **116**, 2417–2424, https://doi.org/10.1175/1520-0493(1988)116<2417:SSBOTM>2.0.CO;2.

Murphy, J., and Coauthors, 2010: Towards prediction of decadal climate variability and change. *Procedia Environ. Sci.*, **1**, 287–304, https://doi.org/10.1016/j.proenv.2010.09.018.

Park, J.-Y., J.-G. Jhun, S.-Y. Yim, and W.-M. Kim, 2010: Decadal changes in two types of the western North Pacific subtropical high in boreal summer associated with Asian summer monsoon/El Niño–Southern Oscillation connections. *J. Geophys. Res.*, **115**, D21129, https://doi.org/10.1029/2009JD013642.

Qian, Y., D. Gong, J. Fan, L. R. Leung, R. Bennartz, D. Chen, and W. Wang, 2009: Heavy pollution suppresses light rain in China: Observations and modeling. *J. Geophys. Res.*, **114**, D00K02, https://doi.org/10.1029/2008JD011575.

Rayner, N. A., D. E. Parker, E. B. Horton, C. K. Folland, L. V. Alexander, D. P. Rowell, E. C. Kent, and A. Kaplan, 2003: Global analyses of sea surface temperature, sea ice, and night marine air temperature since the late nineteenth century. *J. Geophys. Res.*, **108**, 4407, https://doi.org/10.1029/2002JD002670.

Roeckner, E., and Coauthors, 1996: The atmospheric general circulation model ECHAM4: Model description and simulation of the present-day climate. MPI Rep. 218, 90 pp.

Smith, D. M., S. Cusack, A. W. Colman, C. K. Folland, G. R. Harris, and J. M. Murphy, 2007: Improved surface temperature prediction for the coming decade from a global climate model. *Science*, **317**, 796–799, https://doi.org/10.1126/science.1139540.

Smith, T. M., R. W. Reynolds, T. C. Peterson, and J. Lawrimore, 2008: Improvements to NOAA's historical merged land–ocean surface temperature analysis (1880–2006). *J. Climate*, **21**, 2283–2296, https://doi.org/10.1175/2007JCLI2100.1.

——, P. A. Arkin, M. R. P. Sapiano, and C.-Y. Chang, 2010: Merged statistical analyses of historical monthly precipitation anomalies beginning 1900. *J. Climate*, **23**, 5755–5770, https://doi.org/10.1175/2010JCLI3530.1.

Solomon, A., and Coauthors, 2011: Distinguishing the roles of natural and anthropogenically forced decadal climate variability. *Bull. Amer. Meteor. Soc.*, **92**, 141–156, https://doi.org/10.1175/2010BAMS2962.1.

Song, F., T. Zhou, and Y. Qian, 2014: Responses of East Asian summer monsoon to natural and anthropogenic forcings in the 17 latest CMIP5 models. *Geophys. Res. Lett.*, **41**, 596–603, https://doi.org/10.1002/2013GL058705.

Sun, C., J. Li, F.-F. Jin, and R. Ding, 2013: Sea surface temperature inter-hemispheric dipole and its relation to tropical precipitation. *Environ. Res. Lett.*, **8**, 044006, https://doi.org/10.1088/1748-9326/8/4/044006.

Tao, S., and L. Chen, 1987: A review of recent research on the East Asian summer monsoon in China. *Monsoon Meteorology*, C.-P. Chang and T. N. Krishnamurti, Eds., Oxford University Press, 60–92.

Taylor, K. E., R. J. Stouffer, and G. A. Meehl, 2012: An overview of CMIP5 and the experiment design. *Bull. Amer. Meteor. Soc.*, **93**, 485–498, https://doi.org/10.1175/BAMS-D-11-00094.1.

Ueda, H., A. Iwai, K. Kuwako, and M. E. Hori, 2006: Impact of anthropogenic forcing on the Asian summer monsoon as simulated by eight GCMs. *Geophys. Res. Lett.*, **33**, L06703, https://doi.org/10.1029/2005GL025336.

van Oldenborgh, G. J., F. J. Doblas-Reyes, B. Wouters, and W. Hazeleger, 2012: Decadal prediction skill in a multi-model ensemble. *Climate Dyn.*, **38**, 1263–1280, https://doi.org/10.1007/s00382-012-1313-4.

Wang, B., and LinHo, 2002: Rainy season of the Asian–Pacific summer monsoon. *J. Climate*, **15**, 386–398, https://doi.org/10.1175/1520-0442(2002)015<0386:RSOTAP>2.0.CO;2.

——, and Q. Zhang, 2002: Pacific–East Asian teleconnection. Part II: How the Philippine Sea anomalous anticyclone is established during El Niño development. *J. Climate*, **15**, 3252–3265, https://doi.org/10.1175/1520-0442(2002)015<3252:PEATPI>2.0.CO;2.

——, and T. Li, 2004: East Asian monsoon–ENSO interactions. *East Asian Monsoon*, C.-P. Chang, Ed., World Scientific, 177–212.

——, and Q. Ding, 2006: Changes in global monsoon precipitation over the past 56 years. *Geophys. Res. Lett.*, **33**, L06711, https://doi.org/10.1029/2005GL025347.

——, R. Wu, and X. Fu, 2000: Pacific–East Asian teleconnection: How does ENSO affect East Asian climate? *J. Climate*, **13**, 1517–1536, https://doi.org/10.1175/1520-0442(2000)013<1517:PEATHD>2.0.CO;2.

——, ——, and T. Li, 2003: Atmosphere–warm ocean interaction and its impacts on Asian–Australian monsoon variation. *J. Climate*, **16**, 1195–1211, https://doi.org/10.1175/1520-0442(2003)16<1195:AOIAII>2.0.CO;2.

——, I.-S. Kang, and J.-Y. Lee, 2004: Ensemble simulations of Asian–Australian monsoon variability by 11 AGCMs. *J. Climate*, **17**, 803–818, https://doi.org/10.1175/1520-0442(2004)017<0803:ESOAMV>2.0.CO;2.

——, Q. Ding, X. Fu, I.-S. Kang, K. Jin, J. Shukla, and F. Doblas-Reyes, 2005: Fundamental challenge in simulation and prediction of summer monsoon rainfall. *Geophys. Res. Lett.*, **32**, L15711, https://doi.org/10.1029/2005GL022734.

——, Z. Wu, J. Li, J. Liu, C.-P. Chang, Y. Ding, and G. Wu, 2008a: How to measure the strength of the East Asian summer monsoon. *J. Climate*, **21**, 4449–4463, https://doi.org/10.1175/2008JCLI2183.1.

——, J. Yang, T. Zhou, and B. Wang, 2008b: Interdecadal changes in the major modes of Asian–Australian monsoon variability: Strengthening relationship with ENSO since the late 1970s. *J. Climate*, **21**, 1771–1789, https://doi.org/10.1175/2007JCLI1981.1.

——, J. Liu, H.-J. Kim, P. J. Webster, and S.-Y. Yim, 2012: Recent change of the global monsoon precipitation (1979–2008). *Climate Dyn.*, **39**, 1123–1135, https://doi.org/10.1007/s00382-011-1266-z.

——, ——, ——, ——, ——, and B. Xiang, 2013: Northern Hemisphere summer monsoon intensified by mega-El Niño/Southern Oscillation and Atlantic multidecadal oscillation. *Proc. Natl. Acad. Sci. USA*, **110**, 5347–5352, https://doi.org/10.1073/pnas.1219405110.

——, J.-Y. Lee, and B. Xiang, 2015a: Asian summer monsoon rainfall predictability: A predictable mode analysis. *Climate Dyn.*, **44**, 61–74, https://doi.org/10.1007/s00382-014-2218-1.

——, B. Xiang, J. Li, P. J. Webster, M. N. Rajeevan, J. Liu, and K.- J. Ha, 2015b: Rethinking Indian monsoon rainfall prediction in the context of recent global warming. *Nat. Commun.*, **6**, 7154, https://doi.org/10.1038/ncomms8154.

——, and Coauthors, 2018: Toward predicting changes in the land monsoon rainfall a decade in advance. *J. Climate*, **31**, 2699–2714, https://doi.org/10.1175/JCLI-D-17-0521.1.

Wang, T., H. J. Wang, O. H. Otterå, Y. Q. Gao, L. L. Suo, T. Furevik, and L. Yu, 2013: Anthropogenic agent implicated as a prime driver of shift in precipitation in eastern China in the late 1970s. *Atmos. Chem. Phys.*, **13**, 12 433–12 450, https://doi.org/10.5194/acp-13-12433-2013.

WMO, 2002: Standardised verification system (SVS) for long-range forecasts (LRF): New attachment II-9 to the manual on the GDPS. WMO 485, 23 pp.

Wu, B., R. Zhang, B. Wang, and R. D'Arrigo, 2009: On the association between spring Arctic sea ice concentration and Chinese summer rainfall. *Geophys. Res. Lett.*, **36**, L09501, https://doi.org/10.1029/2009GL037299.

Wu, R., and B. Wang, 2002: A contrast of the East Asian summer monsoon–ENSO relationship between 1962–77 and 1978–93. *J. Climate*, **15**, 3266–3279, https://doi.org/10.1175/1520-0442(2002)015<3266:ACOTEA>2.0.CO;2.

——, and B. P. Kirtman, 2005: Roles of Indian and Pacific Ocean air–sea coupling in tropical atmospheric variability. *Climate Dyn.*, **25**, 155–170, https://doi.org/10.1007/s00382-005-0003-x.

Xing, W., B. Wang, and S.-Y. Yim, 2016: Peak-summer East Asian rainfall predictability and prediction. Part I: Southeast Asia. *Climate Dyn.*, **47**, 1–13, https://doi.org/10.1007/s00382-014-2385-0.

Yang, F., and K.-M. Lau, 2004: Trend and variability of China precipitation in spring and summer: Linkage to sea-surface temperatures. *Int. J. Climatol.*, **24**, 1625–1644, https://doi.org/10.1002/joc.1094.

Yim, S.-Y., B. Wang, and M. Kwon, 2014a: Interdecadal change of the controlling mechanisms for East Asian early summer rainfall variation around the mid-1990s. *Climate Dyn.*, **42**, 1325–1333, https://doi.org/10.1007/s00382-013-1760-6.

——, ——, and W. Xing, 2014b: Prediction of early summer rainfall over South China by a physical-empirical model. *Climate Dyn.*, **43**, 1883–1891, https://doi.org/10.1007/s00382-013-2014-3.

Yoon, J., and S.-W. Yeh, 2010: Influence of the Pacific decadal oscillation on the relationship between El Niño and the northeast Asian summer monsoon. *J. Climate*, **23**, 4525–4537, https://doi.org/10.1175/2010JCLI3352.1.

Yu, L., T. Furevik, O. H. Otterå, and Y. Gao, 2015: Modulation of the Pacific decadal oscillation on the summer precipitation over east China: A comparison of observations to 600-years control run of Bergen Climate Model. *Climate Dyn.*, **44**, 475–494, https://doi.org/10.1007/s00382-014-2141-5.

Zhang, R., 2015: Natural and human-induced changes in summer climate over the East Asian monsoon region in the last half century: A review. *Adv. Climate Change Res.*, **6**, 131–140, https://doi.org/10.1016/j.accre.2015.09.009.

——, B. Wu, P. Zhao, and J. Han, 2008: The decadal shift of the summer climate in the late 1980s over eastern China and its possible causes. *J. Meteor. Res.*, **22**, 435–445.

Zhao, P., S. Yang, and R. Yu, 2010: Long-term changes in rainfall over eastern China and large-scale atmospheric circulation associated with recent global warming. *J. Climate*, **23**, 1544–1562, https://doi.org/10.1175/2009JCLI2660.1.

Zhou, T., D. Gong, J. Li, and B. Li, 2009a: Detecting and understanding the multi-decadal variability of the East Asian summer monsoon recent progress and state of affairs. *Meteor. Z.*, **18**, 455–467, https://doi.org/10.1127/0941-2948/2009/0396.

——, and Coauthors, 2009b: Why the western Pacific subtropical high has extended westward since the late 1970s. *J. Climate*, **22**, 2199–2215, https://doi.org/10.1175/2008JCLI2527.1.

Zhu, C., B. Wang, W. Qian, and B. Zhang, 2012: Recent weakening of northern East Asian summer monsoon: A possible response to global warming. *Geophys. Res. Lett.*, **39**, L09701, https://doi.org/10.1029/2012GL051155.

Zhu, Z., and T. Li, 2017: Empirical prediction of the onset dates of South China Sea summer monsoon. *Climate Dyn*. **48**, 1633–1645, https://doi.org/10.1007/s00382-016-3164-x.

——, J. He, and L. Qi, 2012: Seasonal transition of East Asian subtropical monsoon and its possible mechanism. *J. Trop. Meteor.*, **18**, 305–311.

——, T. Li, and J. He, 2014: Out-of-phase relationship between boreal spring and summer decadal rainfall changes in southern China. *J. Climate*, **27**, 1083–1099, https://doi.org/10.1175/JCLI-D-13-00180.1.